INTERNATIONAL JOURNAL FOR NUMERICAL METHODS IN FLUIDS
Int. J. Numer. Meth. Fluids 2006; **50**:235–253
Published online 7 September 2005 in Wiley InterScience (www.interscience.wiley.com). DOI: 10.1002/fld.1052

A study of the recirculating flow in planar, symmetrical branching channels

Yeng-Yung Tsui*,† and Chih-Yu Lu‡

Department of Mechanical Engineering, National Chiao Tung University, Hsinchu 300, Taiwan, R.O.C.

SUMMARY

A numerical method is employed to examine the flow in symmetrical, two-dimensional branches of Y shape and Tee shape. The methodology is based on a pressure-correction procedure within the frame of unstructured grids. Specified pressures are imposed at the outlets of the two branches. The area ratio of the branch is allowed to vary in the range of 2–3. Separation of the flow in the bifurcating region is inevitable. With equal outlet pressures, symmetrical flow patterns prevail except for the Y type branch under the conditions of high Reynolds numbers and large area ratios. This implies that the Y-branch flow is more sensitive to small disturbances. It is shown that with a slightly higher pressure imposed on one of the two branches the structure of the recirculating flow for the Y type is greatly affected and the flow rate is reduced dramatically in the high-pressure branch channel. In contrast, the influence on the Tee type branch is much lower since the flow behaves like a jet impinging on a confined duct.

KEY WORDS: branching flows; recirculating vortices; symmetry breaking; pressure boundary conditions; unstructured grids

1. INTRODUCTION

The flow through branching channels has been widely used in industrial applications, such as piping systems and ventilation systems, and is encountered in human bodies. When fluid passes the branch junction, it changes direction, leading to skew axial velocity profiles, separation and secondary flows. These flow characteristics are implicated to be a main factor to the pollutants deposition in human respiratory system. The vascular system depends on the branches to distribute blood. The arterial walls in the branching regions are exposed to high and low

*Correspondence to: Yeng-Yung Tsui, Department of Mechanical Engineering, National Chiao Tung University, Hsinchu 300, Taiwan, R.O.C.
†E-mail: yytsui@mail.nctu.edu.tw
‡E-mail: yytsui@cc.nctu.edu.tw

Contract/grant sponsor: National Science Council of the R.O.C.; contract/grant number: NSC 91-2212-E-009-051

Received 28 April 2005
Revised 10 June 2005
Accepted 10 June 2005

shear stresses which disturb local mass transfer and cause cell degradation. Therefore, the atherosclerosis occurs mainly in these regions.

A most popular model used to study the bifurcating flows is a 90° Tee junction, i.e. a straight channel with a branch offset at 90°. Karino *et al.* [1] adopted a particle suspension technique to identify that when part of the flow is diverted into the branch channel, it becomes inevitable for the flow to separate from the corner of the junction and a recirculation zone is formed unless the Reynolds is sufficiently low. Another recirculation vortex may also appear along the outer wall of the main channel near the bifurcation region. The sizes of the two recirculation zones depend on either the Reynolds number or the flow diversion ratio, defined as the ratio of the flow rate through the side branch to the total flow rate. The two-vortex pattern is the most common to see, which covers a wide range of diversion ratio. At extremely high diversion ratios of values greater than 0.9 for $Re > 100$, three vortices were found by Karino *et al.* The third vortex, which is much smaller than the second one, is located at the inner wall of the main channel downstream of the second one. Although the above observation made by Karino *et al.* was obtained in tubing ducts, similar flow patterns could be found in channel flows with rectangular cross-sections [2, 3] and in planar, two-dimensional calculations [2, 4, 5]. In the study of Liepsch *et al.* [2] both the laser Doppler anemometry (LDA) measurements in a test rig with an area ratio of 8:1 and the corresponding 2-D calculations indicated that with $Re = 515$ and diversion ratio of 0.23 there is no separation in the main channel. By increasing the diversion ratio to 0.44 with $Re = 496$, a recirculation zone could be seen. Three-dimensional calculations conducted by Neary and Sotiropoulos [3] revealed that, in comparison with 2-D calculations, closer agreement with the measurements of Liepsch *et al.* was achieved in the recirculation region in the branch channel. This implies that the vortex flow there is mainly three-dimensional, rather than two-dimensional. The third vortex formed in the main channel at high diversion ratios was captured in the predictions by Khodadadi *et al.* [4]. They also showed that the sizes of the two recirculation zones increase with the increasing Reynolds number. However, as the diversion ratio increases, there exists a peak size value for the recirculating vortices. Travers and Worek [6] examined the flow in Tee junctions with the branch protruding into the main duct using a computational method. It was shown that the protrusion intensifies the local pressure drop in the branch region and leads to a greater overall pressure loss. It is common to specify flow split between the branches as a boundary condition in calculations. In addition to this type of boundary condition, the study by Hayes *et al.* [5] also considered the boundary condition of equal pressures at the two branch outlets. For the case with equal pressures the fractional flow in the main duct increases with increasing Reynolds number. The critical Reynolds number at which the first recirculation zone appears in the side branch increases with increasing diversion ratio and with decreasing side branch width. The flows with side branches other than 90° have also been investigated. Both the computations by Kawaguti and Hamano [7] and the experimental work by Cho *et al.* [8] indicated that the flow patterns are similar to those for the 90° Tee junctions.

In this study the flows in planar (two-dimensional), symmetrical branches are under investigation. Two different bifurcation geometries are examined: a symmetrical Y branch with 90° branching angle and a symmetrical Tee branch (180° branching angle). The main difference between two- and three-dimensional flows lies in that secondary velocities in the transverse directions are induced in the 3-D flow, which complicates the flow in the streamwise

direction [9, 10]. However, the problems in 2-D are of interest because features such as separation, attachment and flow reversal predominate the flow structure.

By surveying the literature it is rather surprising that there are only a few works concerning the symmetrical bifurcation. In the early work of Lynn *et al.* [11] a 60° Y branch was examined. The area ratio, defined as the total cross-sectional area of the daughter channels downstream of the bifurcation to the area of the main channel upstream, was set at 1. The results indicated that there is no flow separation in the daughter branches. Bramley and Dennis [12] considered a Y branch with an angle of 90°. The flow with a small area ratio of $1/\sqrt{2}$ does not separate whereas in the wide daughter ducts (area ratio $=\sqrt{2}$) flow separation occurs for $Re > 100$. The sharp corners of the branch used by Bramley and Dennis [12] were smoothed out in a later study [13]. It was found that the corner shape has little effects on the flow patterns. The influence of branching angle was also checked to find that the tendency to separate increases with the angle. However, the results showed that the angle does not change the size of the recirculation zone significantly. El-Shaboury *et al.* [14] reported a study of forced convection through a symmetrical Tee branch with area ratio of 2 for a wide range of split flow ratio β. For equal split ratio ($\beta = 0.5$) the flow is symmetrical and a recirculation zone was found in each of the daughter channel. For split ratio not equal to 0.5 a second vortex may be seen downstream of the main vortex along the opposite wall, depending on the Reynolds number and the split ratio. The corresponding vortices in the two daughter channels are not of equal size. The recirculating flow strongly influences the distribution of the shear stress and the wall heat flux. The condition of equal split ratio was found to produce maximum overall heat transfer and minimum pressure drop. Lou and Yang [15] examined the blood flow in a 2-D, symmetrical, aortic bifurcation. The arterial walls were assumed to be rigid. No permanent recirculating vortices were found in the pulsatile flow. But a temporary recirculation region exists under certain conditions, for example, at a large area ratio. There are no fundamental differences in the flow structure between the Newtonian and non-Newtonian models [16]. The effect of wall flexibility of the artery was accounted for in another study by Lou and Yang [17]. It was revealed that the wall expansion tends to induce flow reversals during the decelerating systole, while contraction tends to restrict them during the diastole. In the above works the flows were assumed to be two-dimensional. A three-dimensional numerical study for the flow in a symmetrical bifurcation with an area ratio of 2.0 and a branch angle of 60° was reported by Yung *et al.* [9]. It was seen that due to the centrifugal force a secondary vortex flow is induced in the branch. The secondary motion alters the streamwise velocity profiles. A region of reversed flow was observed near the outer wall of the branch except for the case of the lowest Reynolds number. An experimental investigation using the LDA was carried out by Rieu *et al.* [10] to examine the flow in a symmetrical bifurcation with a rectangular cross-section of area ratio 0.8 and various branch angles. The features such as the secondary vortex flow, the shift of the maximum streamwise velocity towards the inner wall, and the recirculation zone along the outer wall of the branch could be identified in their results. It was noted that the recirculating vortex is formed at branching angle of 180°, but not detected for branching angles less than 90°.

It can be concluded from the above reviews that the flow is hardly separated in a Y branch with the branching angle less than 90° and an area ratio less than 1. In this study we examine the branching flow with the area ratio in the range of 2–3. At these high area ratios flow reversal becomes inevitable. Two branching angles, 90° and 180°, are under consideration. Unlike the previous studies, in which the computational domain covered only half the flow

domain because the flow was assumed to be symmetrical to the centreline of the main channel, the entire flow domain is considered in the present computations. Another difference is that in most numerical studies the flow rate is designated in each branch duct whereas it is the pressure specified as the outlet boundary condition in this study. It will be seen in our results that with equal exit pressures the flow may become asymmetrical due to the instability embedded in the flow when the area ratio and the Reynolds number become sufficiently large. In addition, we will investigate the effects of slightly different pressures prescribed on the outlets. This is used to mimic the situation of non-exactly symmetrical configurations existing in the real world.

2. MATHEMATICAL METHOD

The equations governing the steady, incompressible flow in dimensionless form are given as

$$\nabla \bullet \mathbf{V} = 0 \tag{1}$$

$$\nabla \bullet (\mathbf{VV}) = -\nabla P + \frac{1}{Re}\nabla^2 \mathbf{V} \tag{2}$$

Here the coordinates and the velocities are normalized using half the inlet width c and the mean velocity $\bar{V}$ averaged over the inlet. The dimensionless pressure and Reynolds number are given as

$$P = \frac{p}{\rho \bar{V}^2} \tag{3}$$

$$Re = \frac{\rho \bar{V} c}{\mu} \tag{4}$$

In the Y branch configuration the two branches are skew to the main channel. To deal with this skew geometry, a usual way is to adopt curvilinear coordinates and a transformation of the coordinates for the governing equations is necessitated. A structured grid can be constructed to cover the entire domain. However, for the Tee branch geometry the grid nodes in the regions next to the main channel become redundant. To avoid grid redundancy, zonal approaches have been proposed [18–20]. By this procedure the grids in the main and the branch channels are generated separately and the solution in each of the zones is sought sequentially. Iteration over these zones must be undertaken to ensure coupling of the flows in the different zones. An alternative way, without requiring solution iteration, is to adopt the unstructured grid. Another merit in using the unstructured grid is that there is no need to make coordinate transformation, which preserves the strong conservation property of the original differential equations. In the following, the methodology suitable for unstructured grids is described briefly. For more details the reader are referred to Reference [21].

The above equations are of divergence form. Integrating the momentum equation over a polyhedral cell of n faces and applying divergence theorem the following discretized equation can be obtained:

$$\sum_{f=1}^{n} (\rho \mathbf{V} \bullet \mathbf{s})_f \phi_f = \sum_{f=1}^{n} (\mu \nabla \phi \bullet \mathbf{s})_f + S \tag{5}$$

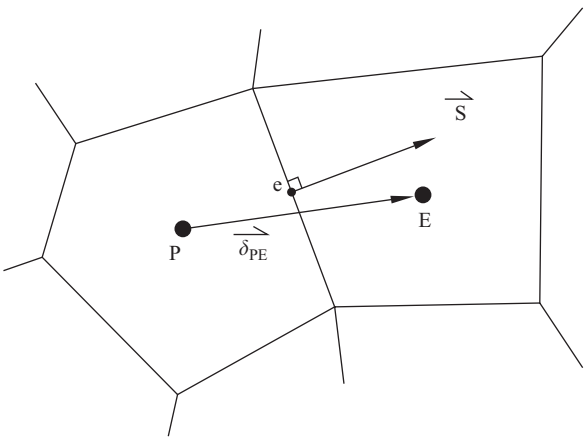

Figure 1. Illustration of a face e between the primary cell P and a neighbouring cell E.

Here the dimensional form is employed and ϕ represents a velocity component. The term on the left-hand side designates the convection flux through face f and the first term on the right-hand side the diffusion flux. The summations are over the n faces. The last term S denotes the volume integral of the pressure gradient.

In the convection flux the face value ϕ_f is estimated by the central difference. An important issue is the determination of the diffusion flux. Consider a face e in Figure 1. Let $\mathbf{s}$ be surface vector of the face and $\boldsymbol{\delta}_{PE}$ be the vector directed from the primary cell node P to the neighbouring cell node E. In the past decade a number of expressions have been proposed to represent the diffusion flux. As shown in Reference [21], these approximations are equivalent to the following form:

$$F_e^d = \frac{\mu_e s^2}{\boldsymbol{\delta}_{PE} \bullet \mathbf{s}}(\phi_E - \phi_P) + \mu_e \overline{\nabla\phi}_e \bullet (\mathbf{s} - \mathbf{d}) \tag{6}$$

where $\mathbf{d}$ is a vector in the direction of $\boldsymbol{\delta}_{PE}$, defined by

$$\mathbf{d} = \frac{s^2}{\boldsymbol{\delta}_{PE} \bullet \mathbf{s}} \boldsymbol{\delta}_{PE} \tag{7}$$

The gradient at the face $\overline{\nabla\phi}_e$ is approximated using interpolation form the two adjacent nodes P and E

$$\overline{\nabla\phi}_e = (1 - f_P)\nabla\phi_P + f_P\nabla\phi_E \tag{8}$$

In the present method the velocity and the pressure are collocated at the cell centres. To enforce mass conservation on each cell, it is needed to calculate the velocity at cell face:

$$\mathbf{V}_e = \overline{\mathbf{V}}_e - (D_e\nabla p_e - D_e\overline{\nabla p}_e) \tag{9}$$

The overbars denote interpolation from the two nodes P and E, similar to Equation (8). The mass flux through the face is then estimated by

$$\dot{m}_e = \bar{\rho}_e \bar{\mathbf{V}}_e \bullet \mathbf{s} - A_E^P[(p_E - p_P) - \overline{\nabla p_e} \bullet \boldsymbol{\delta}_{PE}] \tag{10}$$

where

$$A_E^p = \bar{\rho}_e D_e \frac{s^2}{\boldsymbol{\delta}_{PE} \bullet \mathbf{s}} \tag{11}$$

Following the SIMPLE algorithm of Patankar [22], the correction of mass flux is linearly related to the pressure correction as

$$\begin{aligned} \dot{m}'_e &= -\bar{\rho}_e D_e \nabla p'_e \bullet \mathbf{s} \\ &\approx A_E^p(p'_P - p'_E) - \bar{\rho}_e D_e \overline{\nabla p'_e} \bullet (\mathbf{s} - \mathbf{d}) \end{aligned} \tag{12}$$

Forcing the corrected velocity field to satisfy the continuity constraint leads to a pressure-correction equation.

$$A_P p'_P = \sum_{C=1}^{n} A_C p'_C + S_{p1} + S_{p2} \tag{13}$$

where

$$S_{p1} = -\sum_{f=1}^{n} m_f^* \tag{14a}$$

$$S_{p2} = \sum_{f=1}^{n} \bar{\rho}_f D_f \overline{\nabla p'_f} \bullet (\mathbf{s} - \mathbf{d}) \tag{14b}$$

The S_{p2} term, representing the contribution of the nodes additional to the ones adjacent to the cell faces, is equivalent to the cross derivatives of the pressure gradient when using curvilinear coordinates. It can be shown that this term disappears when the vector $\boldsymbol{\delta}_{PE}$ is in the same direction as the surface vector $\mathbf{s}$ because, then $\mathbf{d}$ becomes identical to $\mathbf{s}$. In the past, this term was totally ignored during solution iteration due to the difficulty to handle these 'corner' nodes in unstructured grid calculations. However, as learned from structured grid experience, neglecting the corner node contribution may deteriorate convergence efficiency if the grid is greatly 'skew'. To take account of this term a successive-correction procedure was employed. It was shown [21] that only two correction steps bring about the most efficient and stable solution.

The solution procedure is similar to that of SIMPLE algorithm. The momentum equation and the pressure-correction equation are solved sequentially. After the pressure correction is yielded, the velocity and the mass flux are upgraded accordingly. The sequence of solution iteration is carried out until convergence criteria are reached.

The boundary condition is assumed to be a fully developed flow at the inlet of the main channel. As for the branch outlets, the pressure boundary condition is imposed. When the

static pressure is specified at the outlet boundary, the mass flux can be calculated in a similar manner as in Equation (10).

$$\dot{m}_{\text{out}} = \bar{\rho}_b(\mathbf{V}_b) \bullet \mathbf{s}_b - \rho_b D_P \frac{s_b^2}{\boldsymbol{\delta}_{Pb} \bullet \mathbf{s}_b}[(p_b - p_P) - \nabla p_b \bullet \boldsymbol{\delta}_{Pb}] \tag{15}$$

The subscript b denotes the boundary node. The boundary velocity is yielded via the first-order extrapolation, namely, $\mathbf{V}_b = \mathbf{V}_P$. The pressure gradient at the boundary can be derived from the following relationship for a variable, say, ϕ:

$$\phi_b - \phi_p = \nabla\phi \bullet \delta_{pb} \approx \frac{1}{\Delta v}\left[\phi_b \mathbf{s}_b + \sum_{f \neq b} \phi_f \mathbf{s}_f\right] \tag{16}$$

where the summation is taken over all the surrounding faces except for the boundary face.

3. VALIDATION TESTS

The method described above is verified for a number of two-dimensional problems including a Y branch and a Tee junction. In addition to the pressure boundary condition, another type of boundary condition, fixed split flow in each branch channel, will be encountered in the validating tests. For this condition the velocities at the exits are adjusted after each solution iteration such that the mass flux in each branch is kept at the specified flow rate.

Case I. Symmetrical Y branch flow: This case has been examined by Bramley and Sloan [13]. The flow was assumed to be symmetrical and, thus, only half the domain was used in their calculations. In the present calculations the entire domain was considered. To ensure flow symmetry one half of the flow rate was enforced on the two exits. For the configuration of area ratio of $\sqrt{2}$ flow separation occurs at the corners where the flow bifurcates. The dependence of the length of the recirculating vortex on the Reynolds number for 60°, 90° and 120° branching angles is shown in Figure 2. It needs to be noticed that the bifurcating corners were smoothed out in the computations of Bramley and Sloan while sharp corners were used in the present study. It is evident from Figure 2 that this difference in the corner geometry has little effect on the vortex length. Flow details reveal that with the sharp corners the separation occurs right at the corners whereas with the corners rounded the separation point is shifted to the location about one half of the inlet width downstream.

Case II. Y branch flow with prescribed pressure boundary condition: The second case considers a 90° Y branch with different pressures specified at the two outlets. The abscissa in Figure 3 represents the pressure difference normalized by $\rho\bar{V}^2/2$. The ordinate is the fraction of the flow rate through the low-pressure branch divided by the total flow rate. Both predictions by the present calculations and by Kelkar and Choudhury [23] indicate a linear relationship between the flow rate and the pressure difference.

The cases tested in the following concern a Tee junction, not the symmetrical Tee branch as will be examined. The Tee junction is made of a straight channel with a perpendicular side branch.

Case III. Tee junction flow with specified flow split condition: For this case the flow rates in the two branches are fixed. The flow is inevitably separated on the inner wall of the side branch. The variation of the reattachment location with the Reynolds number for different

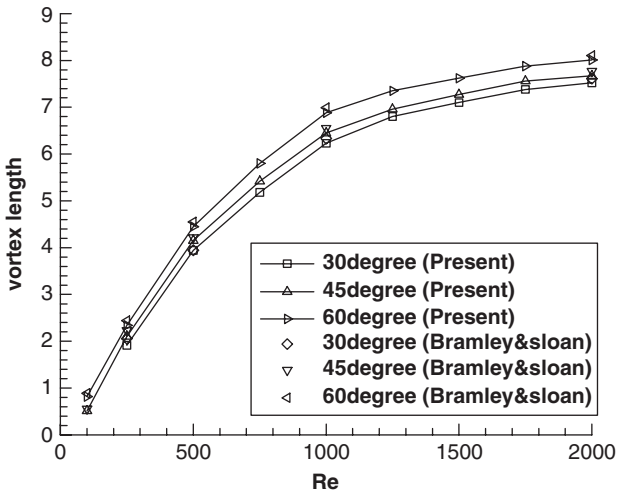

Figure 2. Comparison of the recirculating vortex length in case I with the predictions by Bramley and Sloan.

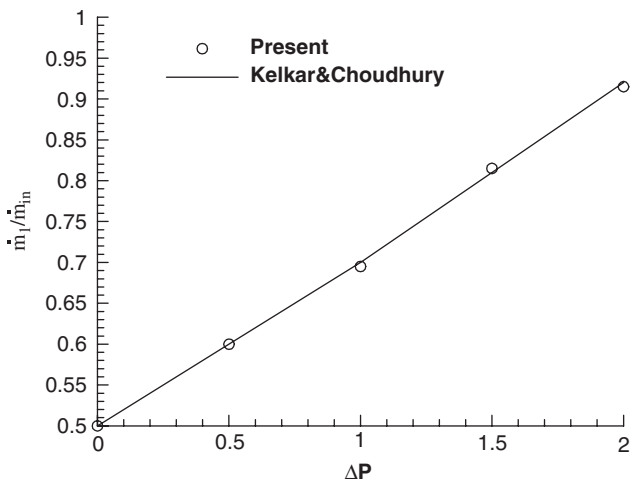

Figure 3. Comparison of the fractional flow rate in case II with the predictions by Kelkar and Choudhury.

split numbers is displayed in Figure 4. The split number is defined as the ratio of the flow rate of the main branch to the total flow rate. Remarkable coincidence with the predictions of Hayes *et al.* [5] is obtained. Further approval of the present method is given in Figure 5 which shows close resemblance in the streamwise velocity profiles at three locations in the separation region between the predictions and the measurements of Liepsch *et al.* [2]. In the figure v is the velocity along the side duct, which is normalized by the mean velocity in this

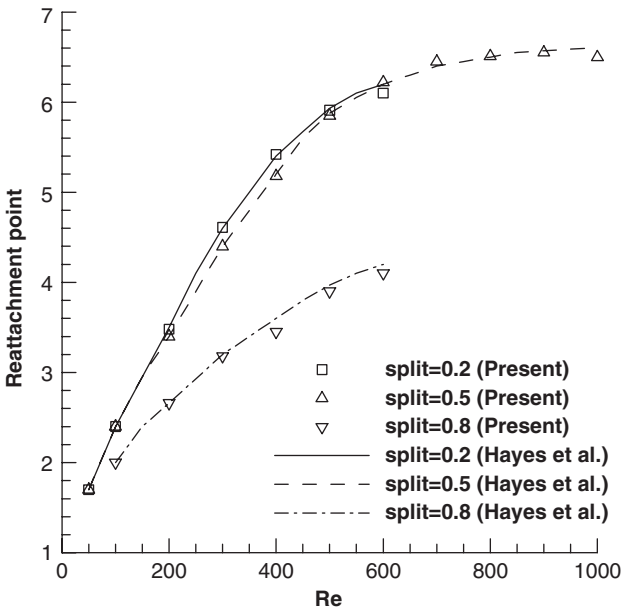

Figure 4. Comparison of the reattachment point in case III with the predictions by Hayes *et al.*

branch V. In this test the flow split is 0.56 and the Reynolds number is 496. The value of 496 is based on the hydraulic diameter for a rectangular duct with an aspect ratio of 8:1. It corresponds to $Re = 140$ when half the inlet width is used as the characteristic length.

Case IV. Tee junction flow with equal exit pressures: For this case equal pressures are prescribed on the exits of the main channel and the side branch. The effects of the Reynolds number on the flow rate of the main branch are presented in Figure 6. The agreement with the predictions of Hayes *et al.* [5] and Kelkar and Choudhury [23] is excellent.

4. RESULTS AND DISCUSSION

The configurations for the Y branch and the Tee branch are shown in Figure 7. It is noted that all the lengths are scaled by half the width of the main channel c. Therefore, the dimensionless width of the branch channels d simply represents the ratio of the total area of the branches to the area of the main channel. The length of the main channel is fixed at 2.5 units while that of the branch channels is in the range of 61–81 units, depending on their width. There are a number of recirculating vortices formed in the branches. As will be seen later, the size of the main vortex in the vicinity of the bifurcating point is within 25 units and the reattachment point of the last vortex will not exceed 40 units. Therefore, there is enough space for the flow to recover from separation and to approach the fully developed state. The choice of grids has been carefully made. The grid is non-uniformly distributed with a larger number of lines clustering in the bifurcation region, which is shown in Figure 8. In the end, the total number

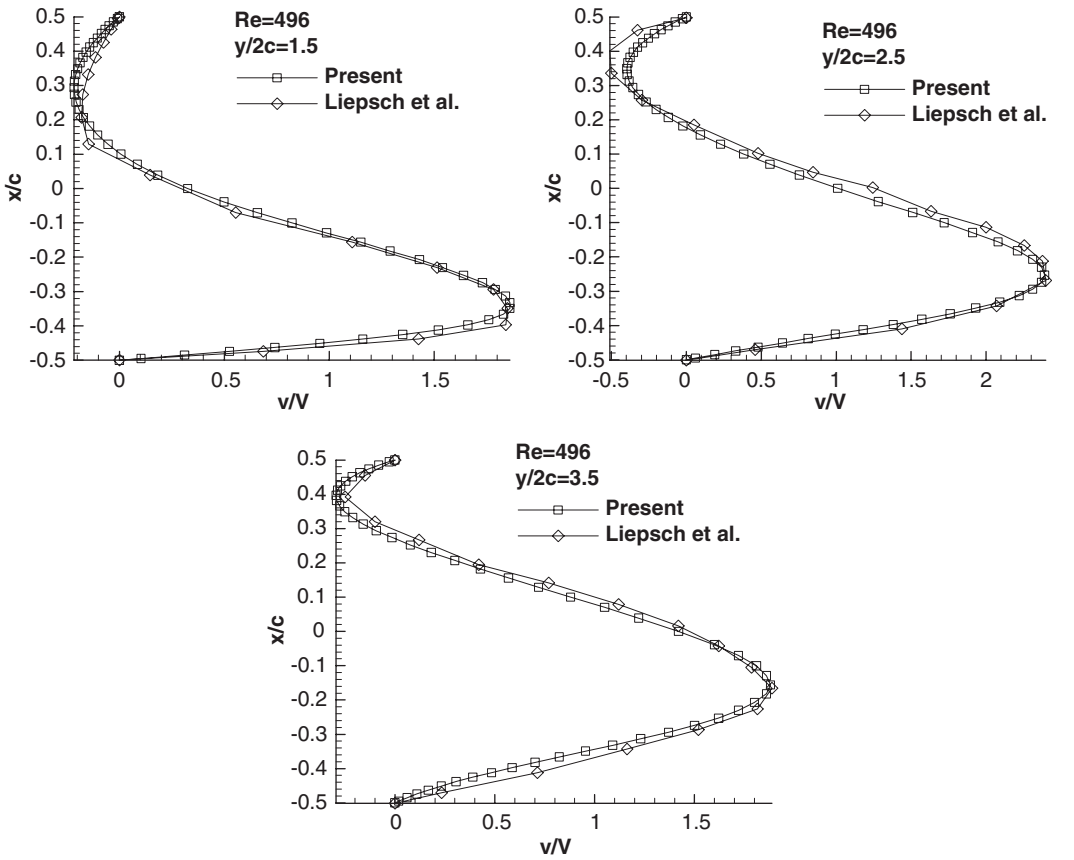

Figure 5. Comparison of the streamwise velocity at three locations in case III with the measurements of Liepsch.

of cells in the streamwise direction ranges from 240 to 280 and the numbers in the normal direction in the branch channels are 20, 25 and 30 (40, 50 and 60 in the main channel) for the cases with channel widths of 2, 2.5 and 3, respectively, for the Y branch whereas the corresponding cell numbers for the Tee branch are about 280–290 in the streamwise direction and 25, 30, 35 in the normal direction. To verify the grids adopted an example of our mesh refinement test results is demonstrated in Figure 9 by showing surface vorticity on the inner wall of the upper branch for the Y branch with $d = 3$ and $Re = 600$. The testing work proceeds in two stages. In the first stage the cell number in the normal direction N_y is gradually increased from 25 to 40 while the total cell number in the streamwise direction is fixed at 340. It is seen from Figure 9(a) that the distributions of the vorticity on the wall surface become nearly identical for $N_y > 28$. In the second stage the number of cells in the streamwise direction N_x is allowed to vary in the range form 240 to 320 with $N_y = 30$. Figure 9(b) shows that the results are almost indistinguishable for $N_x > 280$.

To check the influence of the branch channel width three cases are under consideration: $d = 2$, 2.5 and 3. Equal pressures are imposed at the exits of the two branches.

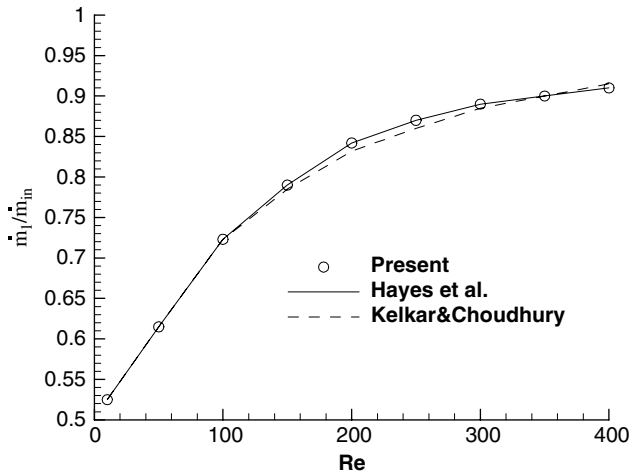

Figure 6. Comparison of the fractional flow rate in case IV with the predictions by Hayes *et al.* and Kelkar and Choudhury.

The characteristic lengths associated to flow separation are shown in Figures 10 and 11 for $d = 2$ and 3, respectively. As seen in Figure 7, X_1, X_3 and X_5 are the lengths of the three recirculating vortices arising in the flow while X_2 and X_4 denote the separation points of the second and the third vortices. For the case with small d of 2 only one recirculating vortex is found at the inner wall downstream of the bifurcation corner in each branch. The size of this vortex is linearly proportional to the Reynolds number for $Re > 100$. When d is enlarged to 2.5 and 3, a weaker vortex is found at the outer wall for the Y branch and, further, a third one at the side of the main vortex in the Tee branch, which is schematically illustrated in Figure 7. The flow patterns in the two branches are identical in the Tee branch since the corresponding characteristic lengths are exactly the same. However, for the Y branch some differences are visible as Re reaches 600 for $d = 2.5$ (not shown in the figure) and 400 for $d = 3$. The asymmetry is believed to be attributed to the flow instability which is often encountered in expansion flows. It has been observed that for the flow through a symmetric diffuser [24, 25] or through a symmetrical sudden expansion [26, 27] there exist two recirculating vortices of different sizes on the two channel walls when the Reynolds number exceeds a critical value. This critical Reynolds number Re_{cr} depends on the expansion ratio; the larger the expansion ratio, the smaller is the Re_{cr}. It is known that blood flows in the vascular system are non-Newtonian. A recent study by Neofytou and Drikakis [28] examined non-Newtonian flows through a symmetric expansion by using three models. It was shown that, similar to Newtonian flows, symmetry breaks at a critical point. This critical point depends on the Reynolds number as well as the specific parameters included in each model. In all the above-mentioned studies the flow was assumed to be steady and two-dimensional. Mallinger and Drikakis [29] have investigated a three-dimensional pulsatile flow in a circular tube with an axisymmetric stenosis. Their simulations revealed that instability initiates inside the stenosis, resulting in a breaking of the flow axisymmetry in a three-dimensional manner. It is generally believed that instability originates from the shear layers separating the main stream and the recirculating

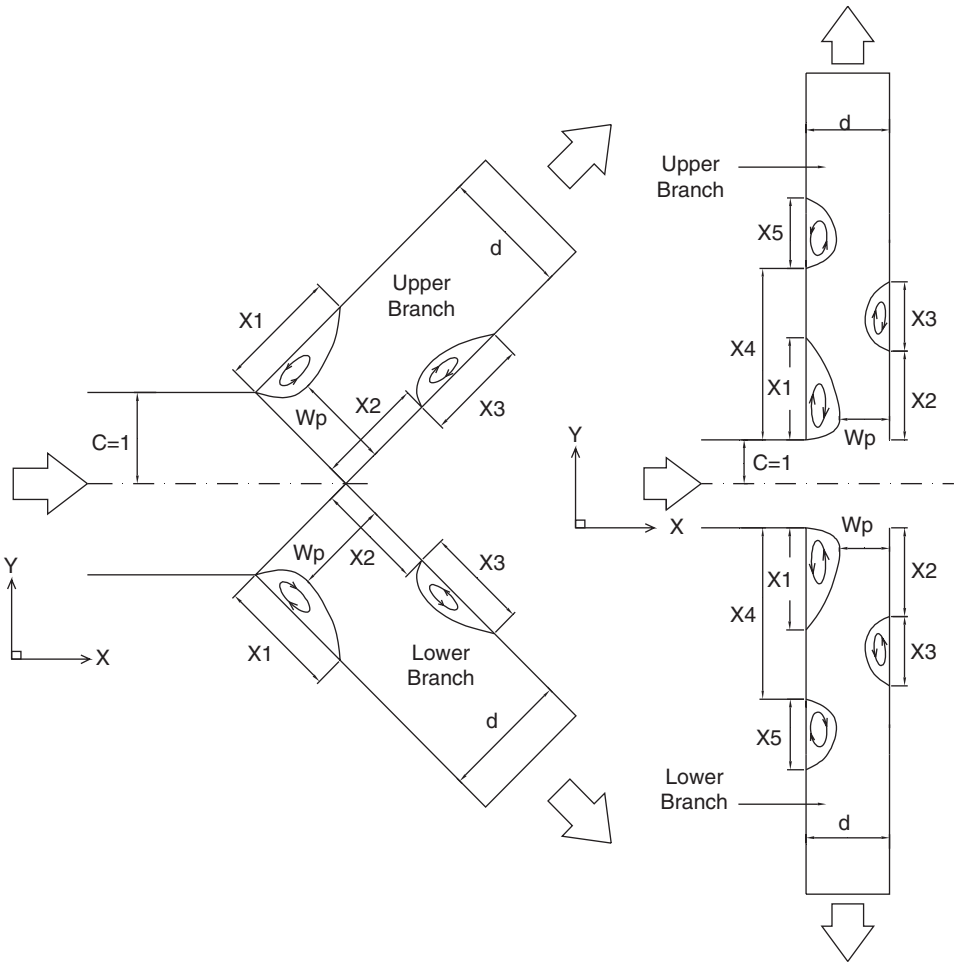

Figure 7. Schematic drawing of the Y and Tee branches.

flows. For sufficiently large Reynolds numbers small disturbances embedded in the shear layer may be amplified to form wavy flows. Due to confinement of the expanded channel the shear layers on the two edges of the incoming jet affect each other, resulting in alternating shedding of vortices and, then, flow asymmetry [30]. In the sudden expansion flow, the difference in the size between the two recirculation zones increases rapidly when the Reynolds number exceeds the critical value. However, as seen in Figure 11(a), the difference is minor in the branching flow. This result can be understood in view of the fact that in the sudden expansion flow the two shear layers are on the two sides of a single main stream whereas each individual layer exists in its own branch in the branching flow. Therefore, the interaction between the two shear layers is intensive for the former; a perturbation occurring in one layer will easily be detected by the other layer. As for the latter, the effect of the perturbation is mostly restricted

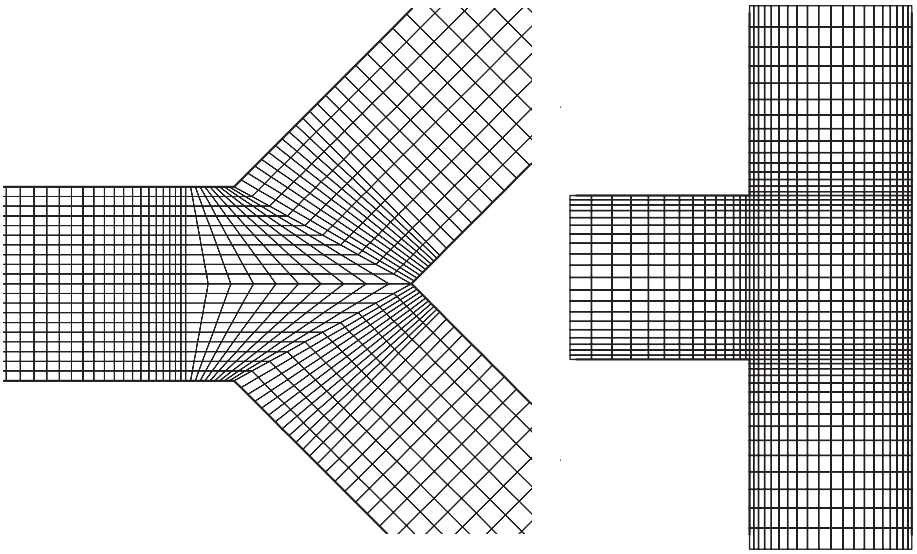

Figure 8. Illustration of the grid arrangement in the bifurcation region.

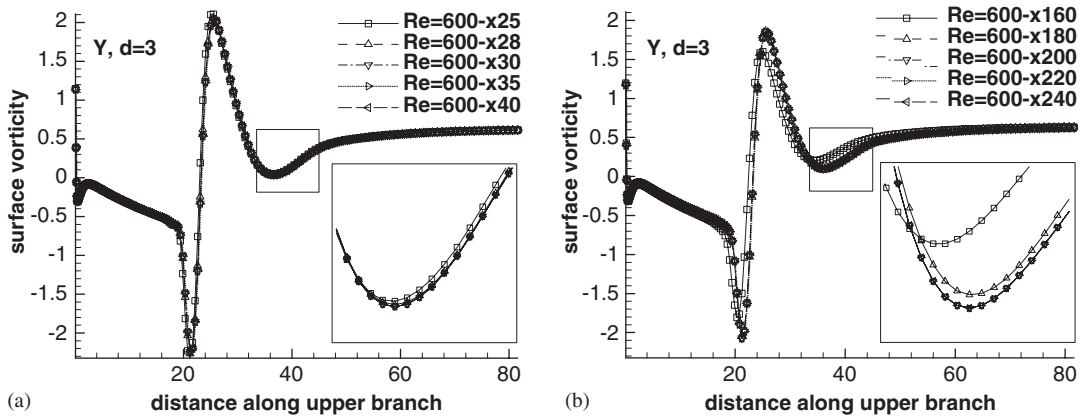

Figure 9. Grid refinement tests for the Y branch flow with $d = 3$ and $Re = 600$: (a) test of N_y; and (b) test of N_x.

in the local branch. To trigger asymmetric flow, asymmetric perturbations in the two branches are required. The asymmetric perturbations can be created via both, as done in the present study, the use of asymmetric linear equation solvers and the round-off errors of the computer itself [31]. In Reference [29] a time-dependent white-noise perturbation was imposed on the inlet velocity to simulate the instability.

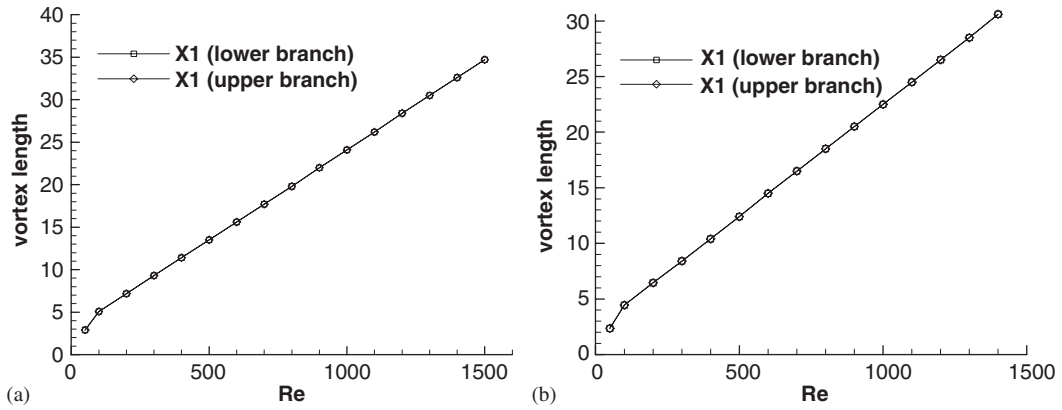

Figure 10. Variation of the characteristic lengths of the vortices for: (a) Y branch; and (b) Tee branch with $\mathrm{d}p = 0$ and $d = 2$.

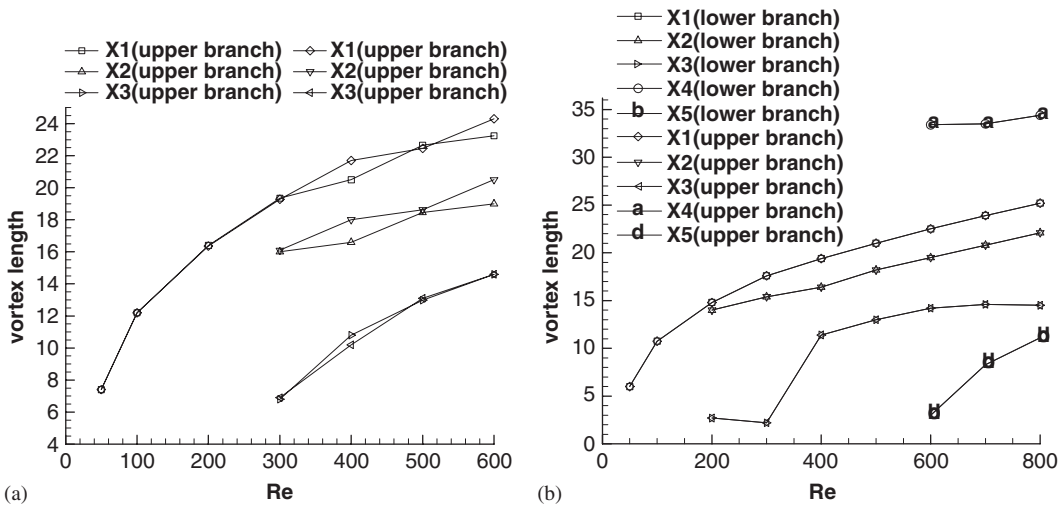

Figure 11. Variation of the characteristic lengths of the vortices for: (a) Y branch; and (b) Tee branch with $\mathrm{d}p = 0$ and $d = 3$.

In practical applications, the configurations of the two branches may not be exactly identical. To mimic this situation, a slight difference between the two exit pressures is allowed. Two pressure differences $\mathrm{d}p = 0.02$ and 0.05 were examined. High pressure level prevails in the lower branch. Figure 12 for $d = 2$ shows that as the Reynolds number increases, the recirculating flows in the two branches gradually differ in size, with a larger vortex in the lower branch and a smaller one in the upper branch. The difference in the lengths of the two vortices in the Tee branch flow is so small that the flow is nearly symmetrical. The linear relationship between vortex length and Reynolds number still exists for large Reynolds

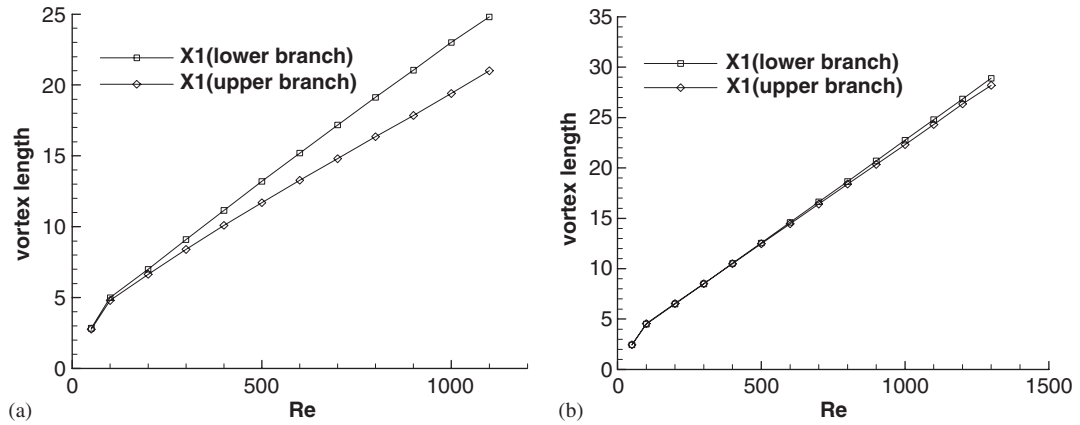

Figure 12. Variation of the characteristic lengths of the vortices for: (a) Y branch; and (b) Tee branch with $dp = 0.05$ and $d = 2$.

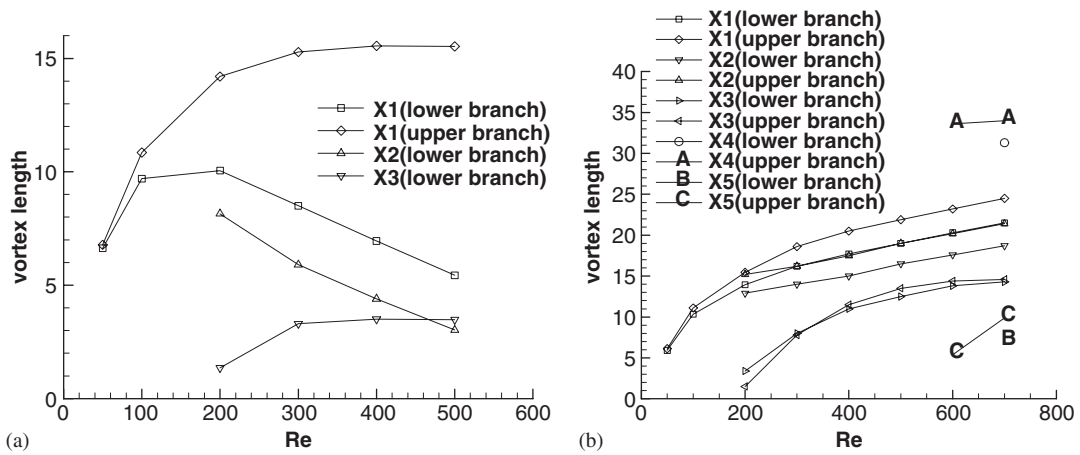

Figure 13. Variation of the characteristic lengths of the vortices for: (a) Y branch; and (b) Tee branch with $dp = 0.05$ and $d = 3$.

numbers. For the Y branch the second vortex in the upper branch, seen in the equal exit pressure case with $d = 2.5$ and 3, disappears, which is shown in Figure 13(a). The second vortex in the upper branch and the third vortex in the two branches altogether vanish in the Tee branch flow for $d = 2.5$ (not shown), but persist for $d = 3$ (see Figure 13(b)). It is noted that, unlike the case with $d = 2$, the main vortex in the upper branch becomes longer than that in the lower branch. Some of the above features can be verified in the streamline plots shown in Figure 14. According to this figure, the flow patterns are not much affected by the appearance of pressure difference for the Tee branch, but it does change the flow structure significantly in the Y branch. In the latter, the second vortex in the upper branch is eliminated and the vortices in the lower branch are greatly shortened and widened. The main vortex enlarged

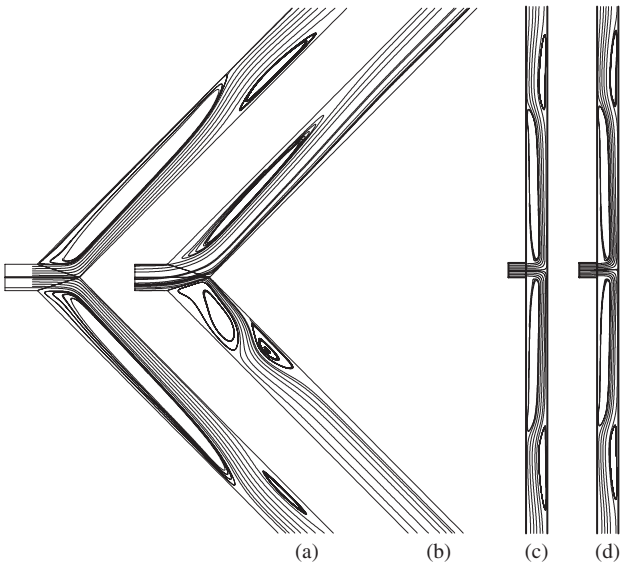

Figure 14. Streamlines for Y branch with $d = 3$, $Re = 400$: (a) $dp = 0$; and (b) $dp = 0.02$; and for Tee branch with $d = 3$, $Re = 600$; (c) $dp = 0$; and (d) $dp = 0.02$.

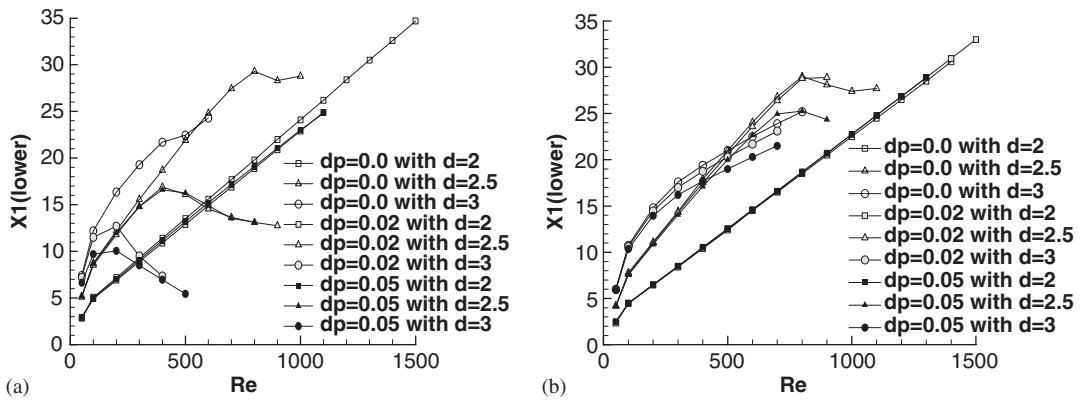

Figure 15. Variation of the main vortex length in the lower branch for: (a) Y branch; and (b) Tee branch.

in the transverse direction blocks the flow passage and results in great impact on the flow rate in the lower branch, as will be seen later. The variation of the main vortex with Re for different configurations in the lower branch is illustrated in Figure 15. The influence of dp is insignificant for the narrow branch with $d = 2$, but not for the cases with d greater than 2, especially in the Y branch flow. In general, the main vortex length is reduced for $d > 2$ as unequal pressure condition is imposed.

It is evident from Figure 16 that less fluid passes through the lower branch as higher pressure is specified. In the figure R is the ratio of the flow rate in this branch to the total

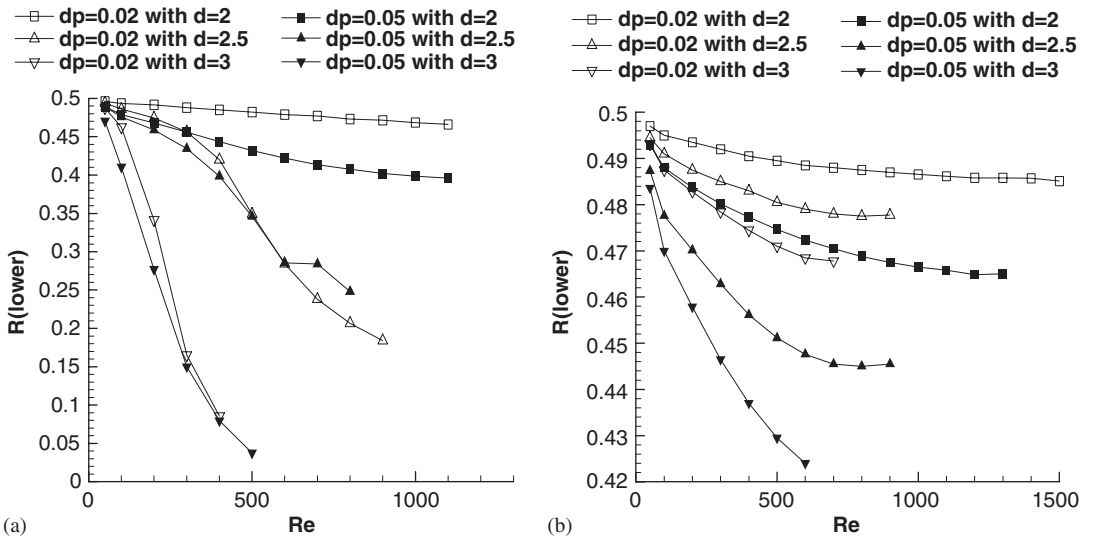

Figure 16. Variation of the flow ratio in the lower branch for: (a) Y branch; and (b) Tee branch.

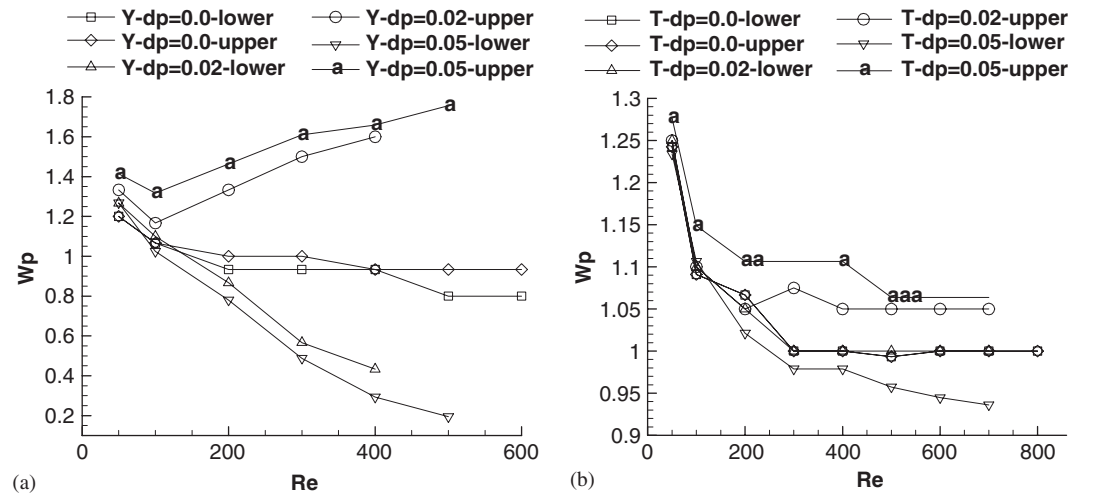

Figure 17. Variation of the passage width in the daughter channels for: (a) Y branch; and (b) Tee branch with $d = 3$.

flow rate. It is noticed that the flow ratio is in the range of 0.4–0.5 for the Tee branch while for the Y branch the flow ratio can drop to less than 0.1 for $d = 3$. This implies that the Tee branch flow is less sensitive to disturbances, which may be attributed to that, as seen in Figure 14, the flow at the bifurcation region behaves like a jet impinging on a confined duct. The jet impingement flow restricts the development of the main vortex in the

transverse direction. For the Y branch flow the enlarged width of the main vortex blockades the passage of the lower branch. This can be verified by examining the passage width W_p, defined as the minimum width of the through-flow passage illustrated in Figure 7, shown in Figure 17 for $d = 3$. The passage width increases with Re in the upper branch for $Re > 100$ and monotonically decreases in the lower branch for the Y branch as different pressures are implemented. As for the Tee branch, although the passage widths in both branches are reduced as Re increases, the decreasing rate for the lower branch is higher than that for the upper branch. Comparing the magnitudes of the passage widths for the two types of branch indicates that this width, along with the flow rate, is greatly affected in the Y branch flow.

5. CONCLUSIONS

A methodology incorporating unstructured meshes and pressure boundary conditions has been developed to examine the flow in branching channels with width $d = 2$, 2.5 and 3. The main findings are summarized in the following:

(1) As equal pressures are specified, the flow in the Tee branch is symmetrical, irrespective of the branch width. However, slightly asymmetrical flow patterns appear at large Reynolds numbers in the Y branch flow for branch area ratio $d \geqslant 2.5$. There is only a main recirculating vortex found in each branch for both types of bifurcation with area ratio $d = 2$. The length of this vortex is, in general, linearly related to the Reynolds number. For larger area ratios, a second vortex can be seen in the Y branch channels and one more vortex in the Tee branch flow.

(2) When a slightly higher pressure is imposed on one of the branches, the flow becomes asymmetrical except at low Reynolds numbers. For $d \geqslant 2.5$ the main vortex in the high-pressure branch becomes shorter, but wider than the one in the low-pressure branch. The increase in the width of this vortex blockades the flow in the high-pressure branch, resulting in decrease of flow rate. Comparing the two types of branch, the Y branch flow is more sensitive to pressure disturbances, leading to a large change in flow pattern and a large variation in flow rate between the two daughter channels. The flow in the Tee branch can be regarded as a jet impingement flow, which has a higher capability to resist disturbances.

ACKNOWLEDGEMENTS

Part of the work was supported by the National Science Council of the R.O.C. under the Contract NSC 91-2212-E-009-051.

REFERENCES

1. Karino T, Kwong HHM, Goldsmith HL. Particle flow behaviour in models of branching vessels: I. vortices in 90° T-junctions. *Biorheology* 1979; **16**:231–248.
2. Liepsch D, Moravec S, Rastogi AK, Vlachos NS. Measurements and calculation of laminar flow in a ninety degree bifurcation. *Journal of Biomechanics* 1982; **15**:473–485.
3. Neary VS, Sotiropoulos F. Numerical investigation of laminar flows through 90-degree diversions of rectangular cross-section. *Computers and Fluids* 1996; **25**:95–118.
4. Khodadadi JM, Nguyen TM, Vlachos NS. Laminar forced convective heat transfer in a two-dimensional 90° bifurcation. *Numerical Heat Transfer* 1986; **9**:677–695.

5. Hayes RE, Nandakumar K, Nasr-El-Din H. Steady laminar flow in a 90 degree planar branch. *Computers and Fluids* 1989; **17**:537–553.
6. Travers TG, Worek WM. Laminar fluid flow in a planar 90 degree bifurcation with and without a protruding branching duct. *Journal of Fluids Engineering* (ASME) 1996; **118**:81–84.
7. Kawaguti M, Hamano A. Numerical study on bifurcating flow of a viscous fluid. *Journal of the Physical Society of Japan* 1979; **46**:1360–1365.
8. Cho YI, Back LH, Crawford DW. Experimental investigation of branch flow ratio, angle, and Reynolds number effects on the pressure and flow fields in arterial branch models. *Journal of Biomechanical Engineering* (ASME) 1985; **107**:257–267.
9. Yung CN, De Witt KJ, Keith Jr TG. Three-dimensional steady flow through a bifurcation. *Journal of Biomechanical Engineering* (ASME) 1990; **112**:189–197.
10. Rieu R, Pelissier R, Farahifar D. An experimental investigation of flow characteristics in bifurcation Models. *European Journal of Mechanics B* 1989; **8**:73–101.
11. Lynn NS, Fox VG, Ross LW. Computation of fluid-dynamical contributions to atherosclerosis at arterial bifurcations. *Biorheology* 1972; **9**:61–66.
12. Bramley JS, Dennis SCR. The numerical solution of two-dimensional flow in a branching channel. *Computers and Fluids* 1984; **12**:339–355.
13. Bramley JS, Sloan DM. Numerical solution for two-dimensional flow in a branching channel using boundary-fitted coordinates. *Computers and Fluids* 1987; **15**:297–311.
14. El-Shaboury AMF, Soliman HM, Ormiston SJ. Laminar forced convection in two-dimensional impacting tee junctions. *Heat and Mass Transfer* 2003; **39**:815–824.
15. Lou Z, Yang W-J. A computer simulation of the blood flow at the aortic bifurcation. *Biomedical Materials and Engineering* 1991; **1**:173–193.
16. Lou Z, Yang W-J. A computer simulation of the non-Newtonian blood flow at the aortic bifurcation. *Journal of Biomechanics* 1993; **26**:37–49.
17. Lou Z, Yang W-J. A computer simulation of the blood flow at the aortic bifurcation with flexible walls. *Journal of Biomechanical Engineering* (ASME) 1993; **115**:306–315.
18. Dimitriadis C, Leschziner MA. Computation of three-dimensional duct junction flow by a zonal approach. *Proceedings of the 4th International Conference on Numerical Methods in Laminar Turbulent Flow*, Swansea, 1985.
19. Koutmos P, McGuirk JJ. Turbofan forced mixer/nozzle temperature and flow field modeling. *International Journal of Heat and Mass Transfer* 1989; **32**:1141–1153.
20. Zhu J, Rodi W. Zonal finite-volume computations of incompressible flows. *Computers and Fluids* 1991; **20**: 411–420.
21. Tsui Y-Y, Pan Y-F, Jung S-P. A pressure-correction method for unstructured meshes with arbitrary polygons. *Proceedings of 10th National Conference CFD*, Hua-Lien, 2003.
22. Patankar SV. *Numerical Heat Transfer and Fluid Flow*. McGraw-Hill: New York, 1980.
23. Kelkar KM, Choudhury D. Numerical method for the prediction of incompressible flow and heat transfer in domains with specified pressure boundary conditions. *Numerical Heat Transfer B* 2000; **38**:15–36.
24. Tsui Y-Y, Wang C-K. Calculation of laminar separated flow in symmetric two-dimensional diffusers. *Journal of Fluids Engineering* (ASME) 1995; **117**:612–616.
25. Shapira M, Degani D, Weihs D. Stability and existence of multiple solutions for viscous flow in suddenly enlarged channels. *Computers and Fluids* 1990; **18**:239–258.
26. Fearn RM, Mullin T, Cliffe KA. Nonlinear flow phenomena in a symmetric sudden expansion. *Journal of Fluid Mechanics* 1990; **211**:595–608.
27. Drikakis D. Bifurcation phenomena in incompressible sudden expansion flows. *Physics of Fluids* 1997; **9**: 76–87.
28. Neofytou P, Drikakis D. Non-Newtonian flow instability in a channel with a sudden expansion. *Journal of Non-Newtonian Fluid Mechanics* 2003; **111**:127–150.
29. Mallinger F, Drikakis D. Instability in three-dimensional, unsteady, stenotic flows. *International Journal of Heat and Fluid Flow* 2002; **23**:657–663.
30. Cherdron W, Durst F, Whitelaw JH. Asymmetric flows and instabilities in symmetric ducts with sudden expansions. *Journal of Fluid Mechanics* 1978; **84**:13–31.
31. Tsui Y-Y, Shu S-J. Effects of buoyancy and orientation on the flow in a duct preceded with a double-step expansion. *International Journal of Heat and Mass Transfer* 1998; **41**:2687–2695.

